UHASSELT
KNOWLEDGE IN ACTION

Maastricht University

Faculty of Medicine and Life Sciences
School for Life Sciences
Master of Biomedical Sciences

Master's thesis

Development and optimization of foundational techniques for the characterization of cytochrome bo3 quinol oxidase from E-coli

Willem Paques

Thesis presented in fulfillment of the requirements for the degree of Master of Biomedical Sciences, specialization Molecular Mechanisms in Health and Disease

SUPERVISOR :

Dr. Ye GAO

2024
2025

Transnational University Limburg is a unique collaboration of two universities in two countries: the University of Hasselt and Maastricht University.

UHASSELT
KNOWLEDGE IN ACTION

www.uhasselt.be
Universiteit Hasselt
Campus Hasselt:
Martelarenlaan 42 | 3500 Hasselt
Campus Diepenbeek:
Agoralaan Gebouw D | 3590 Diepenbeek

Maastricht University

Faculty of Medicine and Life Sciences
School for Life Sciences
Master of Biomedical Sciences

Master's thesis

Development and optimization of foundational techniques for the characterization of cytochrome bo3 quinol oxidase from E-coli

Willem Paques

Thesis presented in fulfillment of the requirements for the degree of Master of Biomedical Sciences, specialization Molecular Mechanisms in Health and Disease

SUPERVISOR :

Dr. Ye GAO

UHASSELT *Senior internship- 2nd master BMW*

Refinement of foundational techniques for characterizing cytochrome *bo*$_3$ quinol oxidase from E. *coli**

Paques Willem[1], Mathew Anjusha[2], and Gao Ye[3]

[1]*Faculty Medicine and Life Sciences, Biomedical Research Institute, Universiteit Hasselt, Campus Diepenbeek, Agoralaan Gebouw C – B-3590 Diepenbeek – Belgium*
[2]*Faculty of Health, Medicine and Life Sciences, Maastricht MultiModal Molecular Imaging Institute - Division of Imaging Mass Spectrometry, Maastricht University, Campus Randwyck, Universiteitssingel 50 – 6229 ER Maastricht – Netherlands*
[3]*Faculty of Health, Medicine and Life Sciences, Maastricht MultiModal Molecular Imaging Institute - Division of Nanoscopy, Maastricht University, Campus Randwyck, Universiteitssingel 50 – 6229 ER Maastricht – Netherlands*

*Running title: *Refining cyt bo*$_3$ *characterization techniques (< 50 characters inc. spaces, italic)*

To whom correspondence should be addressed: Gao Ye, Tel: +31 883 88 78 34; Email: y.gao@maastrichtuniversity.nl

Keywords: Cytochrome *bo*$_3$ oxidase; TM0; E. *coli*; spectrophotometric activity assay; Q Exactive UHMR (hybrid) quadrupole-Orbitrap native-mass spectrometry;

ABSTRACT

Antimicrobial resistance is a major global threat, requiring new therapeutic targets. Prokaryotic cytochrome *bo*$_3$ ubiquinol oxidase (cyt *bo*$_3$) contains a unique transmembrane helix (TM0) involved in substrate/product exchange that represents a druggable site. Structural insights into its conformational dynamics could guide the design of inhibitors that disrupt respiration and kill the host bacterium. Monitoring TM0 charge state dynamics during the redox cycle by native-mass spectrometry (native-MS) may uncover conformational intermediates beyond reported 'open' and 'closed' states.

We overexpressed and purified cyt *bo*$_3$ from Escherichia *coli*, with SDS-PAGE and Blue-Native-PAGE showing characteristic gel bands, while size exclusion chromatography confirmed sample homogeneity. Next, cyt *bo*$_3$ ubiquinol oxidation was measured spectrophotometrically, yielding a turnover rate of 153.91 e$^-$/sec/enzyme (±23.76). Additionally, we optimized native-MS methods to detect cyt *bo*$_3$ on a Q exactive UHMR quadrupole-Orbitrap mass spectrometer. Improved desolvation and ion transmission enabled the detection of a 147,951 Da (±49.01 SD) mass matching the cyt *bo*$_3$ monomer mass from cryo-electron microscopy structures, and a 330,103 Da (±54.38 SD) mass, a putative dimer, respectively. Ion fragmentation using high energy collision induced dissociation to confirm mass identity was unsuccessful, but future strategies will include UV-photodissociation or electron-based fragmentation. Attempts to study ligand-binding effects on TM0's charging status failed due to native-MS signal loss after decylubiquinol addition. Together, these optimized methods enable reproducible cyt *bo*$_3$ detection and activity measurements, providing a foundation for future structural studies of TM0 and its potential as an antimicrobial target.

Commented [WP1]: 25 pages max incl figures/tables
Upload: 01/06/2025

Commented [WP2]: Check if this is fine to use with Ye

Commented [WP3]: Check with Ye if I can use this

Commented [WP4]: 238 words. --> ask for feedback. Worked on rewriting it but I just became really short. This still seems better...

Commented [WP5]: Adjust to chat-GPT comments

INTRODUCTION

Antimicrobial resistance (AMR) occurs when microorganisms evolve to evade or withstand treatment. Overuse of antimicrobials accelerates resistance by killing susceptible strains and allowing resistant ones to thrive (1). AMR is currently the third leading cause of death worldwide, with 1.27 million deaths attributable to bacterial AMR, and Escherichia *coli* (E. *coli*) infections ranked among the top contributors. These infections can cause symptoms like bloody diarrhea or urine, stomach aches, fever, and more (2). Therefore, new antimicrobials targeting essential components for E. *coli's* survival are needed to combat resistant strains. In particular, ATP is critical for cellular growth, motility, nutrient uptake, and overall cellular integrity (3,4). ATP production relies on oxidative phosphorylation, where the electron transport chain establishes a proton gradient, or 'proton motive force', across the membrane that drives many vital processes (5). This project focusses on a key component of E. *coli*'s electron transport chain, the primary terminal oxidase called cytochrome bo_3 ubiquinol oxidase (cyt bo_3). Optimization of methodologies of principal analysis techniques such as spectrophotometric activity assays and native-mass spectrometry will pave the way for upcoming functional and structural characterization of cyt bo_3's active site. Filling this knowledge gap will support future antimicrobial development targeting cyt bo_3.

Cyt bo_3 has a unique TM0 domain – Cyt bo_3 is the primary terminal oxidase expressed by E. *coli* under high oxygen conditions. It is encoded by four genes, *cyoB*, *cyoA*, *cyoC*, and *cyoD*, which produce subunit I (mass: 75 kDa), subunit II (33.5 kDa), subunit III (20.5 kDa), and subunit IV (12 kDa), respectively, and all subunits were reported to be needed for enzymatic activity (6–8). As a member of the heme-copper oxidoreductase superfamily, cyt bo_3 shares strong structural homology with aa_3-type cytochrome *c* oxidases. In particular, subunits I–III are highly conserved, which complicates antimicrobial targeting since effective inhibitors must selectively inhibit the bacterial enzyme without affecting host respiration (8,9). However, subunit I contains an additional transmembrane helix (TM0), consisting of residues 1-41, that is unique to quinol oxidases and absent from the eukaryotic enzyme. Structural studies have shown that TM0 forms a cleft with helices TM1, TM2, and TM3 that constitutes the binding pocket for the substrate ubiquinol-8 (UQH_2). Here, cyt bo_3 catalyzes the two-electron oxidation of UQH_2 to release two protons into the periplasm (Eq. 1) (10,11).

$$UQH_2 + O_{1/2} + 4H^+_{in} \rightleftarrows UQH_0 + H_2O + 4H^+_{out} \quad \text{(Eq. 1)}$$

Additionally, mutagenesis and spectroscopy studies confirmed the functional involvement of four residues in subunit I TM1 (R71, D75) and TM2 (H98, and Q101) in the substrate binding and oxidation (9,12–14). The precise mechanism by which TM0 regulates substrate turnover has remained a long-standing question, motivating ongoing structural and functional studies.

Open and closed TM0 conformations – Recently, structures of cyt bo_3 reconstituted in different membrane mimetics, surfactant and surfactant-like systems that stabilize membrane proteins outside the native bilayer, have been reported using cryo-electron microscopy (cryo-EM). The first structure resolving a UQH_2 molecule in the binding site using cyt bo_3 assembled in SMA-nanodisc (PDB ID: 7CUW, 7CUQ, 7CUB) or MSP-nanodiscs (7N9Z) showed TM0 in a "closed" conformation. In this closed state, TM0 clamps the hydrophobic tail of UQH_2 against a groove between TM1 and TM3, clearly blocking substrate exit. Additionally, the interaction between UQH_2 and the above-mentioned residues in TM1 and TM2 are visualized. Residues R71 and D75 (TM1) hydrogen bonded with the carbonyl O1 oxygen from UQH_2. Notably, residue H98 (TM2) is modeled in two conformations: one positioned to hydrogen bond to the carbonyl O4 oxygen from UQH_2 (reported distance 2.4 Å to the carbonyl, 4.4 Å to E14) and another oriented toward residue E14 (TM0) at the periplasmic end of TM0 (7.3 Å to the carbonyl of UQH_2, 3.1 Å to E14). This spatial arrangement suggested a plausible proton transfer route from UQH_2 to the bulk periplasm via an H98–E14 relay, indicating TM0 involvement not only in the substrate/product exchange, but also in the UQH_2 oxidation (14).

In contrast, a peptidisc-assembled cyt bo_3 structure recently reported by our group captured TM0 in a U-shaped "open" conformation rotated away from

Commented [WP6]: Some figures still need to be added

Commented [WP7]: references

the binding site. In this model, no UQH_2 was observed and residues H98 and R71 adopted positions distinct from the closed state, consistent with an open binding site state. In the closed conformation, TM0 projects inward, positioning E14 near H98 at the periplasmic side, whereas in the open U-shaped form, TM0 folds outward, placing E14 farther from H98 near the bulk environment which supports the involvement of TM0's E14 in the proton shuttling. This outwards folding created space for substrate entry and product release. The extensive spatial movement between closed and open conformations implies the existence of intermediate states during the catalytic cycle. Here, the repositioning of H98, D75, and R71, supports the idea that the open U-shaped conformation represents a substrate-accessible state (9).

Other assemblies, including those prepared in DDM detergent, MSP-nanodiscs, SMA-nanodiscs, and amphipols, consistently yielded the closed conformation (PDB ID's 7XMD, 6WTI, 7CUW, 8F68, respectively) (14–17). Comparison of electron density maps revealed that in these closed structures, additional density from the assemblies overlapped with the space occupied by TM0 in the open U-shaped state (9). This observation suggests that the mimetic environment can affect TM0 conformational freedom, potentially giving bias to the closed TM0 conformation. Further structural and functional comparisons across assemblies are therefore needed to distinguish intrinsic TM0 dynamics from assembly-induced effects.

Approach of the study: Kinetics – To investigate the structure–function characteristics of cyt *bo*$_3$ TM0, we applied a combination of native mass spectrometry (Native-MS) and Michaelis–Menten kinetic analysis. Characterization of enzyme kinetics across different cyt *bo*$_3$ assemblies can provide insight into how these assemblies affect TM0 dynamics and catalytic function. Maximum catalytic capacity (V_{max}) reflects the upper limit of substrate turnover, and differences in V_{max} between assemblies may indicate whether assembly components physically restrict the rotational freedom of TM0, limiting the enzyme's maximum activity. The Michaelis constant (K_m), defined as the substrate concentration at which the reaction rate reaches half of V_{max}, serves as an inverse measure of substrate affinity; changes in K_m across assemblies could indicate that certain mimetics alter accessibility of the binding site, influencing substrate association. The catalytic constant (k_{cat}) presents the intrinsic turnover efficiency of cyt *bo*$_3$ independent of enzyme concentration. If the membrane mimetic restricts TM0 mobility, limiting conformational switching, proton transfer or substrate/product exchange could be slowed, reducing k_{cat}. The k_{cat}/K_m ratio integrates effects on both substrate affinity and turnover, providing a measure of overall catalytic efficiency under low, non-saturating substrate concentrations. Differences in these parameters across assemblies, in combination with the observation that electron density maps of closed TM0 structures contain overlapping densities from assemblies in the space occupied by the open U-shaped TM0, can reveal whether mimetic environments bias conformational states and influence both substrate binding and catalytic efficiency.

Approach of the study: Native-MS – Native-MS can analyze intact protein complexes while preserving their native quaternary structure, enabling top-down characterization of composition, stoichiometry, and non-covalent interactions. Membrane proteins like cyt *bo*$_3$ present challenges for native-MS because their hydrophobicity and tendency to form aggregates require solubilization within membrane mimetics. The critical task is to gently remove these assemblies without disrupting the protein complex. This is accomplished through in-source trapping, which occurs at the very front of the mass spectrometer, right after ion generation but before mass analysis (18).

Here, ions pass sequentially through the S-lens exit lens, the Injection Flatapole, and the Inter-Flatapole lens. Activating in-source trapping adjusts the voltages across these components to create a potential well that temporarily confines the ions, allowing them to collide softly with a small amount of background gas. These mild collisions gently strip away detergent(-like) molecules and other loosely bound particles, effectively desolvating the complex while preserving its integrity (19,20).

Looking ahead, successful detection of cyt *bo*$_3$ through optimized native-MS methodology will provide a foundation for investigating the role of

TM0. Because changes in protein chargeability can be tracked through shifts in charge state distribution, native-MS offers a way to connect structural transitions of TM0 to measurable spectral signatures. Insights from molecular dynamics simulations of the SMA-nanodisc-assembled cyt bo_3 structure support this reasoning: the groove formed between H98 and R71 provides a pathway for water molecules, and comparison with a cyt bo_3 mutant lacking TM0 shows that deletion enlarges this groove, altering its hydrophobicity and water occupancy (14). Additionally, the U-shaped open TM0 conformation was more unfolded than the closed state, influencing the proton accessibility of TM0 residues (9). This potential increase in chargeability of the open conformation might reveal itself in native-MS spectra as increases in charge state distribution, meaning that conformational switching of TM0 could be detected as intermediate states between open and closed conformations.

Research gap and study rationale – Antimicrobial resistance underscores the need for new therapeutic targets. However, the functional role of TM0 in substrate binding, oxidation, and release in cyt bo_3 remains poorly understood, and more structural and functional information is needed to clarify its role. To address this gap, this thesis project focuses on setting up spectrophotometric activity assays to measure the cyt bo_3 substrate oxidation rate, a technique that is new to our lab, and optimize native-MS for the detection of cyt bo_3. In this context, **the research question states**: how does the flexibility of the TM0 domain facilitate substrate and product exchange in the reaction cycle of cyt bo_3? We **hypothesize** that uncovering TM0 conformational intermediates beyond 'open' and 'closed' states can inform therapeutic targeting of cyt bo_3 against antimicrobial-resistant E. *coli*.

EXPERIMENTAL PROCEDURES

Material and instrument manufacturer information are listed in supplementary table S1.

Cyt bo_3 overexpression – E. *coli* C43 (DE3) competent cells were purchased from Thermo Fisher and transformed with a *pET-17b cyoAhisBCDE* plasmid for cyt bo_3 overexpression as described previously (1). This plasmid contains the *cyo* operon with a hexa-histidine tag on the C-terminus of subunit II (*cyoA*) and was gifted by the lab of R. Gennis (21). Transformed cells were grown in LB-Broth Miller medium, supplemented with 30% glycerol, and stored at -80°C. Precultures were grown overnight (shaken, 225 rpm, 37°C) in 10 ml LB medium supplemented with 100 µg/ml ampicillin that was filtered through a 0.45 µm PVDF membrane filter (culture medium).
Inoculation: 2 ml preculture was resuspended in 200 ml culture medium and shaken for 5h (225 rpm, 37°C, OD600 = 3.760).
Upscaling: 108 ml inoculation culture was resuspended in 9 x 1L culture medium and further cultured for 2.25h while shaking (225 rpm, 37°C, OD600 = 0.630).
Protein overexpression was induced with 0.5 mM IPTG followed by overnight incubation (shaking, 130 rpm, 30°C, OD600 = 1.495) and centrifugation (8983g, 5°C, 20 min). The 9 x 1L cultures yielded a total of 20.3 g bacterial pellet.

Protein purification – The bacterial pellets were pooled together and resuspended into 100 ml buffer A (50 mM Tris buffer, pH 8.0, 100 mM NaCl, 10% filtered glycerol) supplemented with 0.01% benzonase and three/100 ml Roche cOmplete™ EDTA-free protease inhibitor tablets. Bacteria were broken by passing them five times through an EmulsiFlex-C3 French Pressure cell (15000-18000 psi, 50 ml/min flow rate), with samples kept on ice between cycles. Cell debris and unbroken bacteria were removed by centrifugation (14,000g, 5°C, 60 min).
Membrane pelleting: Membranes were collected by ultracentrifugation for 2h (208,400g, 4°C) and resuspended into 60 ml buffer A with 1% lauryl maltoside (DDM) and one EDTA-free protease inhibitor. After 3 hours of solubilization (rolling, 4°C), insolubles were removed by ultracentrifugation for 1h (164,700g, 4°C).

Cyt bo_3 purification – The his-tagged cyt bo_3 proteins were purified by immobilized metal affinity chromatography using the HisPur™ Ni-NTA Resin according to the manufacturer's instructions. The column utilizes a resin that consists of agarose beads conjugated to a nickel nitrilotriacetic acid (Ni-NTA). These beads can bind recombinant cyt bo_3 proteins through the His-tag on subunit II. The following steps were all performed at 4°C.

HisPur™ Ni-NTA resin preparation: First, the storage solution (20% ethanol) was removed from the resin through centrifugation at 50g (2 min, 4°C) and washed twice with one column volume (20 ml) miliQ. One column volume of buffer A was then used to equilibrate the resin with 3 rounds of centrifugation (50g, 10 min), removing the top layer of storage solution in between. Chromatography column preparation: Second, The Econo-Column Chromatography column was washed with ~1L miliQ and equilibrated with one column volume of buffer A with 0.02% DDM (buffer B) using gravity-flow. Protein-resin incubation: Third, 60 ml solubilized membrane proteins were supplemented with 5 mM imidazole to reduce non-specific Ni-NTA binding, before incubation (33 rpm, rolling, 4°C, 45 min) with 20 ml equilibrated resin and loaded onto the column. The column was then washed with 10 column volumes of buffer B containing 10 mM imidazole, and 5 column volumes of buffer B with 15 mM imidazole. Proteins were eluted with six column volumes of buffer B supplemented with 250 mM imidazole.

Protein concentrating: Finally, the elutions were concentrated using 30K MWCO Macrosep® Advance Centrifugal Devices. Filter membranes were wet with one column volume (15 ml/tube) miliQ and equilibrated by centrifugation (2150g, 10 min, 8°C) with one column volume of buffer B filtered through a 0.2 µm membrane. Elutions (10 ml each) were loaded on the concentrator tubes and centrifuged (2150g, 8°C) and flow through was collected. This was repeated twice for six elutions total. Imidazole concentration was reduced to < 1 mM with four washing steps using one column volume buffer B and centrifugating (2150g at 8°C) after each step. The concentrated sample was collected by reverse spin and stored at -80°C in 60µl aliquots.

Sample composition assessment – Sample homogeneity was analyzed by size exclusion chromatography (SEC) on a Superose® 6 Increase 3.2/300 column equilibrated in filtered buffer B running with the Shimadzu FPLC system. Purity of the sample was further analyzed by SDS-PAGE and Blue-Native-PAGE. Protein concentration was measured by nanodrop A280 absorbance (BSA-standards).

Decylubiquinone reduction – Decylubiquinone ($dUQH_0$) was reduced in-house and stored at -80°C to prevent partial oxidization before activity measurements. Sodium dithionite was used to reduce $dUQH_0$ on an Extrelut NT1 column as described previously (22). In short, the column was reduced by incubation with $Na_2S_2O_4$ dissolved in nitrogen saturated water (150 mg/ml) for 7 min at room temperature. 10 mg $dUQH_0$ dissolved in 1 ml HPLC-level purity cyclohexane was applied to the reduced column and eluted with 5 ml cyclohexane. Elutes were dried under nitrogen stream and dissolved in 1 ml ethanol (Sigma-Aldrich, Darmstadt, Germany) with 20 mM HCl. ±1 ml reduced $dUQH_2$ was stored in 50 µl aliquots at -80°C.

Spectrophotometry – The Varian Cary® 50 UV-Vis Spectrophotometer was used to measure concentrations spectrophotometrically and perform activity assays.

Concentration determination – $dUQH_2$ concentration dissolved in ethanol was determined by measuring absorption at 290 nm with an extinction coefficient (ϵ) of 4 $mM^{-1}cm^{-1}$ (23). The cyt bo_3 concentration in the stored aliquot samples (buffer B) and native-MS samples (peak SEC fractions in 200 mM ammonium acetate) were quantified using the $A_{560\text{-}580}$ absorbance from the reduced minus oxidized difference spectrum ($\epsilon_{\Delta 560\text{-}580}$ of 24 $mM^{-1}cm^{-1}$) (24). Surplus amount of sodium dithionite was used to reduce cyt bo_3.

Activity assay – The cyt bo_3 oxidase activity was measured spectrophotometrically using the Varian Cary® 50 UV-Vis Spectrophotometer. The oxidation rate of substrate analog $dUQH_2$ was measured with the absorption increase at 275 nm [ϵ = 12.5 $mM^{-1}cm^{-1}$] (25). The activity was measured in 30 mM potassium phosphate buffer (KP_i; pH 7.5) prepared from 5.892 mM K_2HPO_4, 24 mM KH_2PO_4, and supplemented with 0.02% DDM (26). A premix was prepared by adding 120 µM $dUQH_2$ to the KP_i buffer and resuspending well to ensure complete solubilization. 95 µl of the premix was added to 5 µl enzyme (conditions: 2, 0.2, 0.04, or 0.02 µg), or 5 µl KP_i buffer (baseline measurement) to start the reaction. Data represents mean ± standard deviation.

Native-MS preparation – Native-MS analysis of cyt bo_3 (± 1-5 µM) was performed on a Q Exactive UHMR (hybrid) quadrupole-Orbitrap mass spectrometer with a static nano-electrospray ionization (nESI) source and in-house pulled, gold-coated borosilicate capillaries (19,20). Samples

were centrifuged (12000g, 2 min, 4°C) to remove precipitation and buffer exchange to buffer C using SEC. Buffer C contained 200 mM ammonium acetate (pH 6.8, and 0.02% DDM. The SEC plate was stored at 4°C and 3-5 µl/injection of the peak SEC fraction (±1 fraction) was introduced into the capillary for native-MS analysis. Cyt *bo*$_3$ purity and activity in ammonium acetate were assessed as described above.

For native-MS with $dUQH_2$, cyt *bo*$_3$ was concentrated 4:1 by centrifugation (6010g, 20 min, 4°C) using a 10K cutoff Amicon centrifugal filter unit, which was calibrated by centrifugation (6010g, 20 min, 4°C) with 1 column volume buffer B. Cyt *bo*$_3$ (25.7022 µM) was then rebuffered to buffer C using SEC as described above. The peak SEC fraction was diluted 5x with buffer C and centrifuged (12000g, 2 min, 4°C) before preparing the reaction mix and native-MS measurement. The final reaction mix included 0.5816 µM cyt *bo*$_3$, 1.4653 mM $dUQH_2$, and 2.987 mM oxidase inhibitor sodium azide in 200mM ammonium acetate (final concentration 3.076 mM) using a sample:$dUQH_2$:inhibitor ratio of 100:5:2.

All native-MS measurements were performed in positive ion mode using the following settings: scan range = 350-30,000 mass to charge ratio (m/z) with a mass spectral resolution of 2210-8839 (at m/z=200), AGC target = 1e6 or 5e6 ions, maximum injection time = 100-200 ms, capillary spray voltage = 1.4-1.5 kV, inlet capillary temperature = 320°C, S-lens RF level = 200. Each spectrum shows 100-200 scans combined, each containing a single microscan. The noise threshold was set to 3, detector pulsing scheme optimization was set for low m/z transmission, and the RF settings of the transfer ion optics was set to target a high m/z range. To increase protein ion transmission and diminish DDM signal, parameters such as in-source trapping, trapping gas pressure, and DC-offset values of the flatapole, multipoles, and ion transfer lenses were optimized as indicated per spectrum.

The mass spectra were analyzed with Thermo Xcalibur Qual Browser version 4.2.28.14. Spectral deconvolution was performed with UniDec Software V4.1.1. (27). Standard deviation of assigned masses was calculated using ESIprot online (28).

RESULTS

Cyt bo$_3$ *purification and purity analysis* – Optimization of the spectrophotometric activity assay and native-mass spectrometry methodology required substantial quantities of protein. Therefore, cyt *bo*$_3$ was overexpressed in a 9-liter E. *coli* culture yielding 20.3 g bacterial pellet, from which nanodrop A_{280} measurements (BSA-standard) revealed a 140.5 mg protein yield. Size exclusion chromatography fractions containing cyt *bo*$_3$ eluted at 1.57 ml (Fig. 1A). Peak fractions analyzed by SDS-PAGE showed bands migrating to the expected molecular weights for subunits I, II, and III, demonstrating a similar purity as earlier reports (Fig. 1B) (21). Additionally, Blue-Native-PAGE showed a single band around 200 kDa, corresponding to full-length cyt *bo*$_3$, and a band around 330 kDa containing traces of a cyt *bo*$_3$, as determined by LC-MS by a previous student in our group (Fig. 1c).

Spectrophotometry setup –Spectrophotometry setup using the Cary 50 UV-Vis spectrophotometer was initiated prior to this master's thesis project. However, initial attempts produced highly unstable and noisy spectra due to misalignment between the micro-cuvette and the instrument's light beam, which failed to pass through the sample. In collaboration with the IDEE technical department at Maastricht University, a custom adaptor was designed to properly align the sample with the incident aligned. Following this improvement, the cyt *bo*$_3$ concentration of the sample after purification (stock sample) was determined to be 9.2071 µM (Fig. 2) (24).

Activity assay – We tested different cyt bo_3 amounts relative to 120µM $dUQH_2$ in a 100 µl reaction mix to measure steady state $dUQH_2$ oxidation, including 0.2 µg, 0.04 µg, and 0.02 µg enzyme to 120 µM $dUQH_2$ in 100 µl reaction mix (Fig. 3). The corresponding enzymatic turnover rates were 11.02 ±1.59, 39.15 ±7.79, 138.52 ±23.42, and 153.91 ±23.71 e^-/sec/cyt bo_3, respectively (mean ± SD, n = 3, each with paired baseline control). The inverse relationship between enzyme amount and normalized activity suggests that the assay was performed under non-saturating conditions. Additionally, the 0.04 µg and 0.02 µg cyt bo_3 conditions showed a linear absorbance increase indicative of steady state oxidation (Fig. 3A,B). These results confirm the oxidative activity of purified cyt bo_3, and future determination of kinetic parameters (V_{max}, K_m, k_{cat}) will be essential to fully characterize its catalytic properties.

Native-MS sample integrity – Structural analysis of cyt bo_3 TM0 throughout the substrate/product exchange reaction cycle may reveal conformational intermediates. Samples were first rebuffered using SEC, where the peak elution volume (1.6368 ml) exhibited a slight right shift compared to the sample in purification buffer. However, the peak width at half maximal value (FWHM) remained the same for both samples (0.2341 ml FWHM in purification buffer; 0.2152 ml FWHM in ammonium acetate) indicating a comparable level of homogeneity (Fig. 1A). SDS-PAGE and BN-PAGE of peak SEC fractions showed identical band patterns. Finally, the cyt bo_3 activity in ammonium acetate was confirmed from one measurement that yielded a turnover number of 186.85 e^-/sec/cyt bo_3 (using 0.02 µg enzyme, n=1) (table 1).

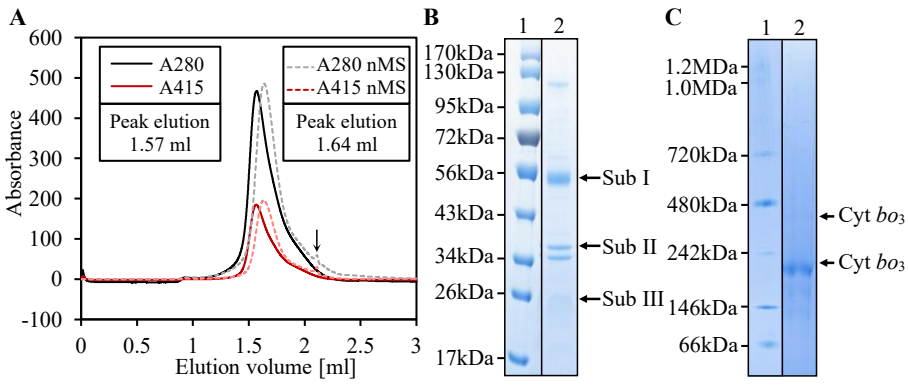

Fig. 1 – Purification of cyt bo_3 ubiquinol oxidase assembled in DDM. (A) Size exclusion chromatography (SEC) profiles of overexpressed cyt bo_3 from a Superose 6 Increase 3.2/300 column at A_{280} (black) and A_{415} (red). Full lines show the profile from stock sample (purification buffer) and dotted lines show native-MS sample in ammonium acetate. The arrow points to a second elution peak in the native-MS profile. Cyt bo_3 subunits and full-length detected by SDS-PAGE (B) and Blue-Native-PAGE (C), respectively. Lane 1 shows the ladder and Lane 2 shows the peak SEC fraction.

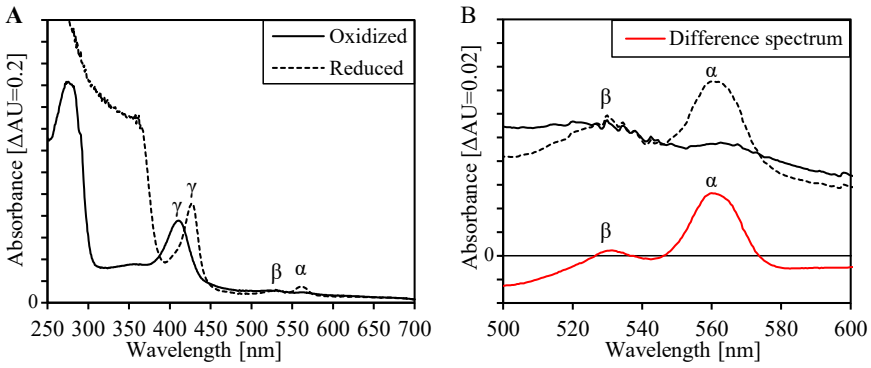

Fig. 2 – Spectroscopic concentration determination of cyt *bo*$_3$.
(A) UV-Vis absorbance spectra of oxidized (solid line) and sodium dithionite-reduced (dotted line) cyt *bo*$_3$ recorded at 23°C using a Cary 50 UV-Vis spectrophotometer (10 mm path length, 60 nm/min scan speed, ~1.5 nm spectral bandwidth). The spectra exhibit spectral features typical of heme-containing oxidases in the Soret (**γ**) band and Q-bands, comprising the **β-** (530 nm) and **α-** (560 nm) bands.
(B) Magnification of the spectrum near the Q-bands showing the reduced-minus-oxidized difference spectrum (red). The relative α-band amplitude (A_{560} minus A_{580}) was used to determine cyt *bo*$_3$ concentration, using an extinction coefficient of 24 $mM^{-1}cm^{-1}$ (24).

Native-MS optimization – Initial native-MS spectra revealed a repeating pattern of peaks separated by a 510 mass-to-charge difference (Δm/z) or its integer fractions. This pattern is characteristic of multiple charge states of DDM oligomers (510 Da monomer) (Fig. 4a). We therefore refined instrument settings step-by-step to detect DDM-assembled cyt bo$_3$ (Fig. 4b-e). First, desolvation of higher mass ions was improved by increasing the desolvation voltage, which deepens the trapping well in the in-source trapping region (injection flatapole) allowing easier protein release from the DDM micelle. Indeed, a low abundance 23+ to 27+ charged peak distribution for a 147,951 Da (±49.01 SD) ion was revealed, closely matching the reported masses from cyt bo$_3$ cryo-EM structures (Fig. 4b) (9,14,16,29). Next, we focused on improving the ion transmission through the in-source trapping region. The DC voltage offsets of the ion directing multipoles in this region were modulated to favor an ion transmission window between 4000-7000 m/z, increasing the abundance of the presumed cyt bo$_3$ peaks (Fig. 4c). Further increasing the desolvation voltage to -250V and the trapping gas pressure removed the remaining DDM signal entirely. It also revealed several other protein peak distributions, e.g. 113 kDa, 199 kDa, 330 kDa, 340 kDa (Fig. 4d). Next, we favored ion transmission towards the m/z range of the 147,951 Da peak distribution using the DC voltage offsets in the in-source trapping region and the C-trap region. Combined with an increased spray voltage, these settings isolated the cyt *bo*$_3$ peak distribution (Fig. 4e).

Tandem native-MS^2 – In literature, peak distributions are conventionally through tandem-MS. In tandem-MS^2, the quadrupole isolates a single peak of interest, and those ions are subsequently fractionated in a high-energy collisional-dissociation cell (HCD) to analyze the resulting peptide fragments. We isolated the 25^+ and 26^+ charge peaks (5919 m/z and 5696 m/z, respectively) from the 147,951 Da peak series to verify it is indeed cyt *bo*$_3$. Figure 5A shows representative native-MS^2 spectra at increasing HCD energies for the 25+ charged peak (±50 m/z). Surprisingly, neither 25+ or 26+ charged peaks fragmented at all, despite a complete loss of precursor ion abundance (Fig. 5A. However, we did observe a minor decrease in the peak m/z values at HCD energies 20eV and 25eV (Fig. 5A). Difficulties in HCD fragmentation are not

Commented [WP8]: Concentration!!!

Table 1 – Turnover rates of cyt bo_3

Cyt bo_3 activity per 120µM $dUQH_2$	2.00 µg	0.20 µg	0.04 µg	0.02 µg
Activity stock sample [e^-/sec/cyt bo_3] (n=3)	11.02 ±1.59	26.58 ±66.88	141.02 ±17.51	153.91 ±23.76
Activity native-MS sample [e^-/sec/cyt bo_3] (n=1)	/	/	/	186.85

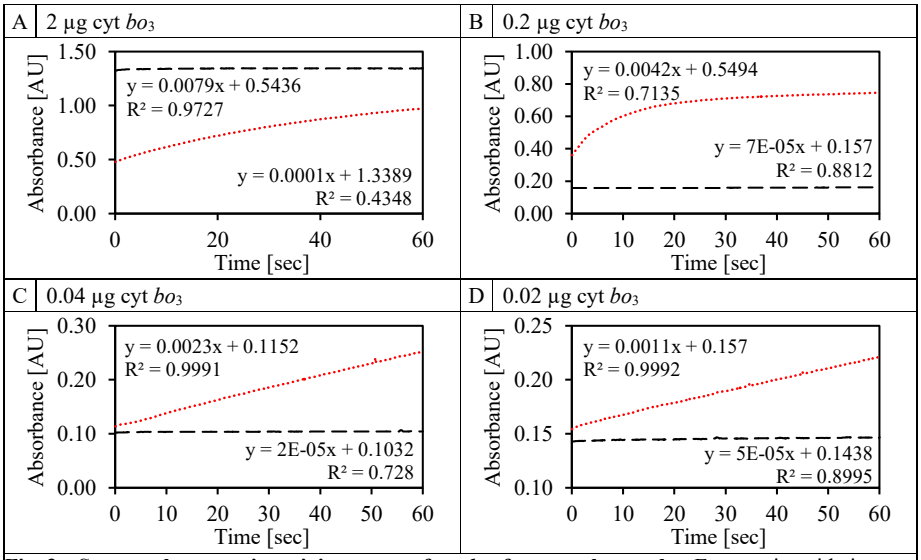

Fig. 3 – Spectrophotometric activity assays of cyt bo_3 from stock samples. Enzymatic oxidation rate of cyt bo_3 measured by monitoring absorbance increase at 275 nm. The slope corresponds to the rate of $dUQH_0$ formation, reflecting cyt bo_3 substrate oxidation. Representative traces are shown for enzyme-containing samples (red) and baseline controls without enzyme (black). Four enzyme concentrations were tested with 120 µM $dUQH_2$ in 100 µl of 30 mM potassium phosphate buffer (pH 7.5) with 0.02% DDM. ***KP_i**, potassium phosphate buffer; **$dUQH_{0/2}$**, decylubiquinone/decylubiquinol.*

uncommon for membrane proteins, but alternative approaches can help overcome these limitations (30).

Alternative mass identification – Next, we analyzed the sample using HCD cell fragmentation without quadrupole isolation. All ions were subjected to stepwise HCD fragmentation from 0 to 50 eV to capture subunit dissociation or fragmentation. No new peak distributions could be found at HCD energies where the presumed cyt bo_3 peak distribution abundance decreased (Fig. 5B). Contrary to the 25 eV HCD energy for isolated peak fragmentation in native-MS^2 experiments, only 14 eV HCD energy was required before the 147,951 Da peak distribution signal fully disappeared (Fig. 5). We suspect mass verification of the presumed cyt bo_3 peak distribution will succeed using alternative fragmentation techniques, though this requires hardware modification and calibration. In the interest of time, we shifted our focus back to the research question.

Towards TM0 analysis – Investigating TM0 conformations throughout the substrate/product exchange cycle first requires detecting the $dUQH_2$-bound cyt bo_3 by native-MS. We applied $dUQH_2$ to the sample and an allosteric activity inhibitor NaN_3 to prevent substrate depletion. These reagents fully abolished the protein signal (Fig. 6). The $dUQH_2$ application was only attempted once due to time constraints and is planned for further optimization. Together with the alternative fragmentation techniques for mass identification, these experiments will further solidify the 147,951 Da

Commented [WP9]: Maybe something about other peaks appearing at the lower m/z values when the 32kDa/ 99kDa signal disappeared?? à find out if those are real masses and what their value is…

Table 2 – Settings of native-MS optimization shown in figure 4.

Settings	Fig. 4a	Fig. 4b	Fig. 4c	Fig. 4d	Fig. 4e/f
Spray voltage	1.2kV	1.2kV	1.2kV	1.2kV	**1.5kV**
Desolvation Voltage	-50V	**-200V**	-200V	**-250V**	-250V
Standardized rapping gas pressure	3	3	3	**5**	5
Injection flatapole DC offset	5V	5V	**7V**	7V	**9V**
Inter flatapole lens DC offset	4V	4V	**5V**	5V	**4V**
Bent flatapole DC offset	2V	2V	**4V**	4V	**1.5V**
Transfer multipole DC offset	0V	0V	0V	0V	**4.3V**
C-trap entrance lens DC offset	1.8V	1.8V	1.8V	1.8V	**3V**
C-trap exit lens DC offset	2V	2V	2V	2V	**6V**

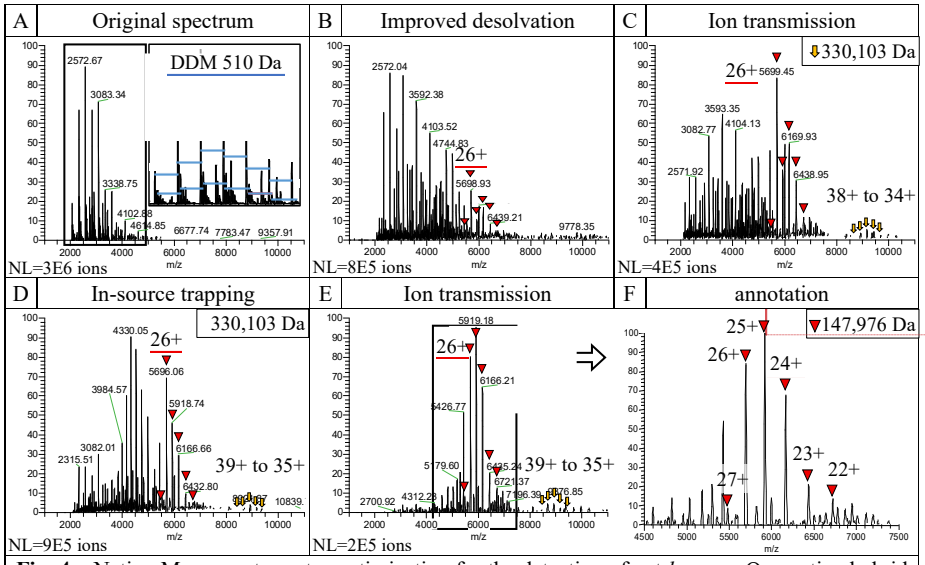

Fig. 4 – Native-Mass spectrometry optimization for the detection of cyt bo_3 on a Q-exactive hybrid quadrupole-orbitrap mass spectrometer. Optimized settings for each figure are shown in table 2.
(A) Original spectrum before optimization showing peaks separated by Δmass-to-charge (m/z) 510 Da, the molecular weight of DDM.
(B-E) Spectra after setting changes as shown in table 2. The 147,951 ±49.01 Da peak series (z = 27+ to 22+ charge states) is suspected to come from cyt bo_3. A 330,103 ±54.38 Da peak series was also detected at lower intensity that might be a cyt bo_3 dimer.
(F) Magnification of spectrum **(E)** showing the charge states of cyt bo_3.
***NL**, Normalization Level (ion abundance at 100%)*

peak series as cyt bo_3 and bring analysis of the TM0 domain closer

DISCUSSION

Protein purification and Homogeneity – The SEC profile of purified cyt bo_3 revealed a single, symmetric peak, indicative of a monodisperse sample. Subsequent analysis by SDS-PAGE and BN-PAGE confirmed that cyt bo_3 is the predominant protein in the preparation, consistent with prior reports (9,21). These results demonstrate that our purification workflow reliably isolates cyt bo_3 in a structurally homogeneous form.

Commented [WP10]: Annotate 130kDa

Commented [WP11]: Question for Ye: is this confusing or does it make sense what I mean with it?

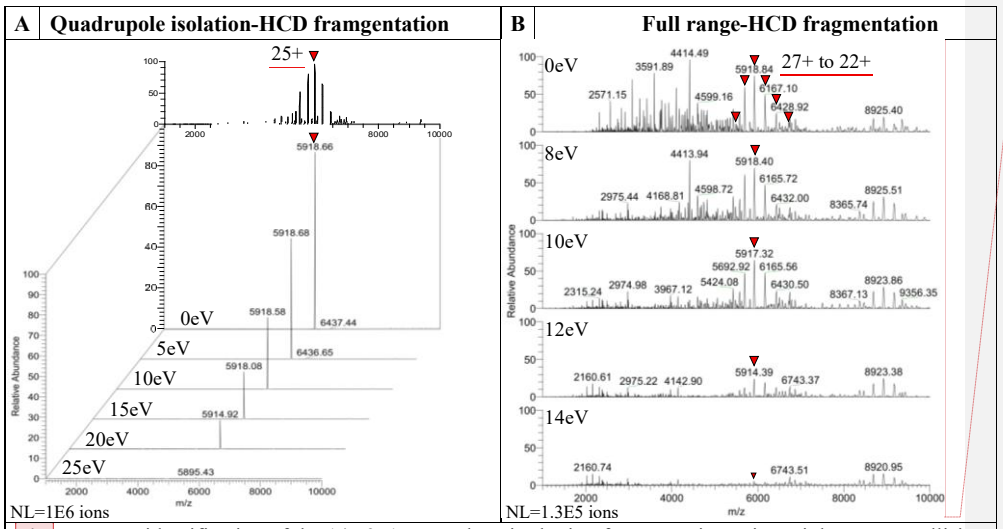

Fig. 5 – Mass identification of the 147,951 Da peak series by ion fragmentation using High-energy Collision induced Dissociation (HCD) energy.
(A) Tandem native-MS (native-MS²) measurements of cyt bo_3 (1.0618 µM) used quadrupole isolation of the 25+ charged peak (5919 ±50 m/z) (red triangle, 0eV) before fragmentation with 5-25eV energy in the HCD cell. Instrument settings from Fig. 4e were used.
(B) Ions were sent to the HCD cell without quadrupole isolation.
m/z*, mass to charge;* ***eV****, electron volts;* ***NL,*** *Normalization Level*

The behavior of cyt bo_3 dissolved in ammonium acetate was also analyzed. First, SEC was conducted using ammonium acetate as the mobile phase, which is widely employed in native-MS due to its volatility and minimal adduction to protein ions. The rightward shift in the peak elution volume compared to the purification buffer sample (from 1.5696 mL in purification buffer to 1.6368 mL), suggests a change in the protein–detergent complex size. The origin of this shift is not certain, but it could arise from changes in micelle behavior or protein folding under low-ionic-strength conditions (31). Detergent micelles, such as DDM, are known to adjust their aggregation number in response to ionic strength, potentially affecting the hydrodynamic radius of the protein–detergent assembly (32). Despite this shift, the SEC peak remained symmetric, indicating that sample homogeneity was preserved.

Purity and homogeneity analysis of the peak SEC fractions from native-MS sample revealed patterns identical to those observed in the purification buffer, indicating that both the primary and quaternary structures of cyt bo_3 were preserved in ammonium acetate, in addition to its activity (Fig. 1A, Table 2). This supports the interpretation that despite the small differences in peak elution volume, the structure and function of cyt bo_3 in activity assay samples and native-MS samples are comparable.
This structural preservation was mirrored in functional assays: activity measurements of cyt bo_3 in ammonium acetate solution (native-MS sample) showed comparable turnover rates to standard buffer conditions, confirming that the enzyme retained its catalytic competence

Kinetic Characterization of Cyt bo_3 – The optimal condition (0.02 µg enzyme with 120 µM $dUQH_2$) yielded a turnover of 153.91 e^-/sec/cyt bo_3. Although our measured turnover rate (153.91 e^-/sec/cyt bo_3) was below previously reported maxima, the established workflow provides a reliable foundation for kinetic comparisons across

Commented [WP16]: Settings used → put in

Commented [WP17]: Ye comment: I won't put the activity assay and concentration determination together in the same photo. Concentration determination belongs to part of purification or yield. Your activity assay should be together with the turnover numbers. Since you did a serie of enzyme concentration, maybe it is also good to create a graph for the different turnover number along with different enzymes used for the activity assay. Also check your method if you described how you made the baseline. You should describe how the baseline was measured if you have it in your results. I think you also compared the activity with purification buffer and ammonium acetate. You are not planning to show the results? The same for your concentration measurement, you are not planning to show the difference between nanodrop and spectrophotometer? These are all your results and you should show them.

Commented [WP18]: In-progress

Commented [WP12]: Verify

Commented [YG13]: Do you have this result in your result session? Make sure the turnover number of activity in two solutions are shown as one result if you want to discussion or conclude here.

Commented [WP14R13]: See comment above.
I did not notice I had activity in AmAc double. Do you think it should be discussed with the other AmAc things (like it is above) or does it fit better in this section with the rest of the activity assay discussion?

Commented [YG15R13]: It is also fine if you want to have a separate discussion on AmAc.

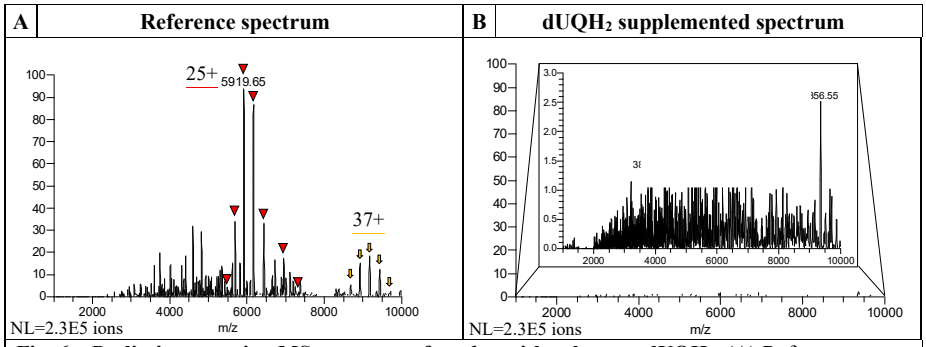

Fig. 6 – Preliminary native-MS spectrum of cyt *bo*$_3$ with substrate dUQH$_2$. (A) Reference spectrum of cyt *bo*$_3$ before substrate supplementation. The peaks belonging to the 147,951 Da species (cyt *bo*$_3$ monomer) are annotated with red triangles, and the 330,103 Da species (cyt *bo*$_3$ dimer) with orange arrows. Each species shows the charge state of the most abundant peak. **(B) S**pectrum of cyt *bo*$_3$ (0.5816 µM) in 200 mM ammonium acetate supplemented with 1.4653 mM dUQH$_2$ in ethanol, and 2.987 mM oxidase inhibitor sodium azide in water. The supplementation reduced ion transmission to <2% of the reference spectrum.
***NL**; normalization level*

different assemblies. Such comparisons can assess whether TM0 rotational freedom contributes to catalysis. Structures from assemblies like DDM, SMA, and amphipols have consistently shown TM0 in the closed conformation, possibly due to steric restriction from the mimetic environment. Future kinetic characterization (V_{max}, K_m, k_{cat}) of cyt *bo*$_3$ reconstituted in DDM, peptidiscs, and alternative assemblies will clarify whether these structural differences correlate with altered turnover or substrate affinity.

Structural and conformational insights from native-mass spectrometry – To detect cyt *bo*$_3$ in its intact form, we first optimized in-source trapping to release the protein complex from its assembly without causing extensive unfolding. The charge state distributions (CSD) from the native MS spectra provided an important structural readout. Narrow distributions with low charge states indicated that cyt *bo*$_3$ maintained a compact, folded conformation, whereas broad, high-charge distributions would suggest unfolding. The spectra consistently showed narrow CSDs, confirming that intact cyt *bo*$_3$ was detected under these conditions.

HCD fragmentation – Mass identification of proteins using native-MS typically relies on native-MS², where precursor ions are fragmented to generate peptide ions whose m/z can inform amino acid sequences. In our experiments, isolation of the 148 kDa cyt *bo*$_3$ peak by the quadrupole was successful, but subsequent HCD fragmentation failed to produce detectable peptide fragments, despite complete loss of the precursor ion at 23 eV. Full-spectrum HCD fragmentation yielded similar results. This limitation is likely due to a combination of instrument-specific constraints and protein properties.

One potential explanation lies in the nature of the collision process and energy transfer during HCD fragmentation. In the collision cell, inert gas atoms (argon in our case) transfer energy to the precursor ions through multiple collisions. Due to the protein's intrinsic rotational freedom, this energy can disperse across many bonds, preventing sufficient accumulation to break covalent bonds and generate peptide fragments. Instead, the bonds may bend or stretch rather than cleave. In contrast, weaker non-covalent interactions—such as lipid adducts, ligands, detergents, or solvent molecules—can be disrupted at lower energies, which could explain the decreasing m/z values shown in figure 5A at 20 eV and 25 eV. Charge stripping may also occur but given the relatively high charge states of the 148 kDa peak (22–27+), complete loss of the precursor ion without a noticeable shift in the average charge state is highly unlikely. Therefore, charge stripping cannot

account for the observed decrease in precursor ion abundance in the absence of fragment ions.

A second potential explanation involves the instrument settings limiting fragment detection. Optimization of ion transmission in our experiments reduced signals below ±5000 m/z by adjusting in-source trapping and C-trap voltages to favor high-mass ions. During HCD, low m/z fragments may lack sufficient kinetic energy to overcome potential barriers in the C-trap entrance and exit lenses, reducing their detection. Other unknown transfer losses from the HCD cell to the C-trap could also contribute. However, even considering this effect, it is unlikely to fully account for the failed nMS^2 experiments, because fragments in the detectable m/z range should still appear if they were produced in sufficient abundance. Other unknown losses during transfer from the HCD cell to the C-trap, or C-trap to orbitrap may contribute but are expected to play a minor role.

Alternative fragmentation methods such as UVPD, ETD, or ECD are also often used for native-MS of protein complexes, as they preserve non-covalent interactions and labile modifications while providing complementary structural information. Employing different fragmentation strategies could successfully verify the cyt bo_3 signal.

Supporting the 147,951 Da annotation – Several lines of evidence support the assignment of the 147,951 Da species observed in native-MS to cyt bo_3. First, cyt bo_3 was the most abundant protein in the SEC fractions as confirmed by SDS-PAGE and BN-PAGE, and in parallel, the 147,951 Da species were among if not the most abundant species in native-MS. However, ion transmission efficiency is protein-specific and influenced by hydrophobicity, pH sensitivity, ionization efficiency, and more, so this is not a direct quantitative measure (33). Second, the enzyme was catalytically active in both purification buffer and ammonium acetate, showing functional integrity. Third, BN-PAGE revealed a band around 300-400 kDa containing traces of cyt bo_3. Together with a reported cryo-EM dimer structure of cyt bo_3 assembled, this strongly suggest that the detected 330,103 Da species by native-MS is a dimer of cyt bo_3. Finally, the measured mass closely matches values calculated from annotated cryo-EM structures (DDM: 148.57 kDa, Peptidisc: 150.09 kDa, SMA-nanodisc: 147.34 kDa, Amphipole: 137.62 kDa, MSP-nanodisc: 147.34 kDa). Importantly, these values include not only the polypeptide chain and cofactors (heme *b*, heme o_3, Cu^{2+}) but also varying numbers and types of co-purified lipids. For instance, the amphipole reconstruction contained only a small complement of three 3PE lipids, whereas SMA- and MSP-nanodiscs captured substantially more lipids, with up to 5 and 9 3PE molecules, respectively. The Peptidisc assembly revealed a mixed set of three 3PE and three POV lipids, while DDM micelles retained only a minimal two PEE lipids. These lipid contributions, each in the range of 500 to 800 Daltons per molecule, account for part of the variation in reported structural masses and explain why slightly different experimental preparations converge around but do not identically reproduce the same total molecular weight.

Towards TM0 analysis – We initially attempted to detect the cyt bo_3–$dUQH_2$ complex by native-MS to gain direct insight into substrate binding and potential structural effects, such as changes in mass or charge distribution. No clear protein-ligand signal was observed in this preliminary trial. This outcome was likely caused by a combination of reagent and experimental constraints. Future strategies could include dissolving $dUQH_2$ in an ammonium acetate–ethanol mixture to reduce the final ethanol concentration in the injected sample while increasing substrate concentration to minimize injection volume. These approaches may improve protein signal and facilitate observation of the substrate-bound complex, providing valuable structural information for TM0 analysis.

Future perspectives – Building on this work, future studies will extend kinetic characterization of cyt bo_3 across different membrane mimetics to determine whether structural constraints imposed by assemblies such as DDM, peptidiscs, and SMA-nanodiscs alter catalytic efficiency or substrate affinity. Complementary native-MS experiments will aim to detect substrate-bound states, providing direct insight into quinone binding and TM0 conformational effects. Integrating these approaches with structural data will help clarify

how TM0 flexibility contributes to proton pumping and electron transfer.

CONCLUSION

This study establishes a robust workflow for the purification, structural characterization, and activity assessment of cyt bo_3 using native-MS. The enzyme was shown to remain catalytically competent and structurally intact in ammonium acetate, with SEC, PAGE, and mass spectrometry supporting the assignment of the 147,951 Da species to cyt bo_3. Although HCD fragmentation did not yield peptide ions, complementary evidence from enzyme integrity assessment, activity assays, and comparison with cryo-EM structures confirmed the protein's identity and integrity. Differences in co-purified lipids across assemblies highlight the influence of the membrane mimetic environment on mass and potentially on TM0 conformational flexibility. Together, these results provide a foundation for future investigations into the relationship between membrane mimetics, TM0 structure, and enzymatic function, and may ultimately support the development of antimicrobial strategies that exploit this unique structural feature of cyt bo_3.

REFERENCES

1. Antimicrobial resistance [Internet]. [cited 2025 Jun 5]. Available from: https://www.who.int/news-room/fact-sheets/detail/antimicrobial-resistance?utm_source=chatgpt.com
2. O'Leary K. The global burden of antimicrobial resistance. Nat Med [Internet]. 2022 Feb 8 [cited 2025 Jun 5]; Available from: https://pubmed.ncbi.nlm.nih.gov/35136233/
3. Hara KY, Kondo A. ATP regulation in bioproduction. Microb Cell Fact [Internet]. 2015 [cited 2025 Aug 16];14:198. Available from: http://www.kegg.jp
4. Dunn J, Grider MH. Physiology, Adenosine Triphosphate. StatPearls [Internet]. 2023 Feb 13 [cited 2025 Aug 16]; Available from: https://www.ncbi.nlm.nih.gov/books/NBK553175/
5. Ortega Morente E, Fernández-Fuentes MA, Grande Burgos MJ, Abriouel H, Pérez Pulido R, Gálvez A. Biocide tolerance in bacteria. Int J Food Microbiol [Internet]. 2013 Mar 1 [cited 2025 Aug 16];162(1):13–25. Available from: https://www.sciencedirect.com/science/article/abs/pii/S016816051300007X
6. Nakamura H, Saiki K, Mogi T, Anraku Y. Assignment and functional roles of the cyoABCDE gene products required for the Escherichia coli bo-type quinol oxidase. J Biochem [Internet]. 1997 [cited 2025 Aug 17];122(2):415–21. Available from: https://pubmed.ncbi.nlm.nih.gov/9378722/
7. Chepuri V, Lemieux L, C-T Au D, Gennisg RB. THE JOURNAL OF BIOLOC~CAL CHEMISTRY The Sequence of the cyo Operon Indicates Substantial Structural Similarities between the Cytochrome o Ubiquinol Oxidase of Escherichia coli and the aas-type Family of Cytochrome c Oxidases*. Journal of Biological Chemistry. 1990;265(19):11185–92.
8. Borisov VB, Verkhovsky MI. Oxygen as Acceptor. EcoSal Plus [Internet]. 2015 Oct 23 [cited 2025 Aug 16];6(2). Available from: https://pubmed.ncbi.nlm.nih.gov/26734697/
9. Gao Y, Zhang Y, Hakke S, Mohren R, Sijbers LJPM, Peters PJ, et al. Cryo-EM structure of cytochrome bo3 quinol oxidase assembled in peptidiscs reveals an "open" conformation for potential ubiquinone-8 release. Biochim Biophys Acta Bioenerg [Internet]. 2024 Aug 1 [cited 2025 Jun 2];1865(3). Available from: https://pubmed.ncbi.nlm.nih.gov/38614453/
10. Matsushita K, Patel L, Ronald Kaback H. [11] Purification and reconstitution of the cytochrome o-type oxidase from Escherichia coli. Methods Enzymol [Internet]. 1986 Jan 1 [cited 2025 Aug 18];126(C):113–22. Available from: https://www.sciencedirect.com/science/article/abs/pii/S0076687986260139
11. Anraku Y, Gennis RB. The aerobic respiratory chain of Escherichia coli. Trends Biochem Sci [Internet]. 1987 Jan 1 [cited 2025 Aug 18];12(C):262–6. Available from: https://www.sciencedirect.com/science/article/abs/pii/0968000487901319
12. Abramson J, Riistama S, Larsson G, Jasaitis A, Svensson-Ek M, Laakkonen L, et al. The structure of the ubiquinol oxidase from Escherichia coli and its ubiquinone binding site. Nat Struct Biol. 2000;7(10):910–7.

13. Choi SK, Lin MT, Ouyang H, Gennis RB. Searching for the low affinity ubiquinone binding site in cytochrome bo3 from Escherichia coli. Biochim Biophys Acta Bioenerg. 2017 May 1;1858(5):366–70.
14. Li J, Han L, Vallese F, Ding Z, Choi SK, Hong S, et al. Cryo-EM structures of Escherichia coli cytochrome bo3 reveal bound phospholipids and ubiquinone-8 in a dynamic substrate binding site. Proc Natl Acad Sci U S A. 2021 Aug 24;118(34).
15. Cryo-EM structure of Escherichia coli cytochrome bo3 in DDM detergent. 2023 Aug 30 [cited 2025 Jun 5]; Available from: https://www.wwpdb.org/pdb?id=pdb_00008go3
16. Su CC, Lyu M, Morgan CE, Bolla JR, Robinson C V., Yu EW. A 'Build and Retrieve' methodology to simultaneously solve cryo-EM structures of membrane proteins. Nature Methods 2021 18:1 [Internet]. 2021 Jan 6 [cited 2025 Jul 13];18(1):69–75. Available from: https://www.nature.com/articles/s41592-020-01021-2
17. Guo Y, Karimullina E, Emde T, Otwinowski Z, Borek D, Savchenko A. Monomer and dimer structures of cytochrome bo3 ubiquinol oxidase from Escherichia coli. Protein Science [Internet]. 2023 Apr 1 [cited 2025 Jul 13];32(4):e4616. Available from: /doi/pdf/10.1002/pro.4616
18. Damoc E, Fort K, Reinhardt-Szyba M, Belov M, Makarov A, Viner R, et al. Advancing Native Top-Down MS Analysis of Non-Covalent Protein Complexes: The Q Exactive UHMR Mass Spectrometer.
19. Mathew A, Giskes F, Lekkas A, Greisch JF, Eijkel GB, Anthony IGM, et al. An Orbitrap/Time-of-Flight Mass Spectrometer for Photofragment Ion Imaging and High-Resolution Mass Analysis of Native Macromolecular Assemblies. J Am Soc Mass Spectrom [Internet]. 2023 Jul 5 [cited 2025 Jun 17];34(7):1359–71. Available from: /doi/pdf/10.1021/jasms.3c00053
20. Mathew A, Buijs R, Eijkel GB, Giskes F, Dyachenko A, Van Der Horst J, et al. Ion Imaging of Native Protein Complexes Using Orthogonal Time-of-Flight Mass Spectrometry and a Timepix Detector. J Am Soc Mass Spectrom [Internet]. 2021 Feb 3 [cited 2025 Jun 17];32(2):569–80. Available from: /doi/pdf/10.1021/jasms.0c00412
21. Rumbley JN, Nickels EF, Gennis RB. One-step purification of histidine-tagged cytochrome bo3 from Escherichia coli and demonstration that associated quinone is not required for the structural integrity of the oxidase. Biochimica et Biophysica Acta (BBA) - Protein Structure and Molecular Enzymology [Internet]. 1997 Jun 20 [cited 2025 Apr 25];1340(1):131–42. Available from: https://www.sciencedirect.com/science/article/pii/S0167483897000368
22. Hildur Palsdottir, Carola Hunte. Membrane Protein Purification and Crystallization [Internet]. Hunte Carola, Gebhard von Jagow, Hermann Schagger, editors. Membrane Protein Purification and Crystallization. 2003 [cited 2025 Aug 5]. 197–198 p. Available from: http://www.sciencedirect.com/science/article/pii/B978012361776750005X
23. Ouchane S, Agalidis I, Astier C. Natural Resistance to Inhibitors of the Ubiquinol Cytochrome c Oxidoreductase of Rubrivivax gelatinosus: Sequence and Functional Analysis of the Cytochrome bc1 Complex. J Bacteriol [Internet]. 2002 [cited 2025 Jun 2];184(14):3815. Available from: https://pmc.ncbi.nlm.nih.gov/articles/PMC135180/
24. Puustinen A, Finel M, Haltia T, Gennis RB, Wikström M. Properties of the Two Terminal Oxidases of Escherichia coli. Biochemistry [Internet]. 1991 Apr 1 [cited 2025 Apr 25];30(16):3936–42. Available from: /doi/pdf/10.1021/bi00230a019
25. Zickermann I, Anemuller S, Richter OM, Tautu OS, Link TA, Ludwig B. Biochemical and spectroscopic properties of the four-subunit quinol oxidase (cytochrome ba3) from Paracoccus denitrificans. Biochimica et Biophysica Acta (BBA) - Bioenergetics [Internet]. 1996 Nov 12 [cited 2025 Apr 25];1277(1–2):93–102. Available from: https://www.sciencedirect.com/science/article/pii/S0005272896000862?via%3Dihub
26. Potassium Phosphate Buffer [Internet]. [cited 2025 Aug 5]. Available from: https://www.novoprolabs.com/tools/buffer-preparations-and-recipes/potassium-phosphate-buffer
27. Marty MT, Baldwin AJ, Marklund EG, Hochberg GKA, Benesch JLP, Robinson C V. Bayesian deconvolution of mass and ion mobility spectra: From binary interactions to polydisperse ensembles. Anal Chem [Internet]. 2015 Apr 21 [cited 2025 Jun 17];87(8):4370–6. Available from: /doi/pdf/10.1021/acs.analchem.5b00140

28. Winkler R. ESIprot: A universal tool for charge state determination and molecular weight calculation of proteins from electrospray ionization mass spectrometry data. Rapid Communications in Mass Spectrometry [Internet]. 2010 [cited 2025 Jun 17];24(3):285–94. Available from: https://pubmed.ncbi.nlm.nih.gov/20049890/
29. Nishida Y, Yanagisawa S, Morita R, Shigematsu H, Shinzawa-Itoh K, Yuki H, et al. Identifying antibiotics based on structural differences in the conserved allostery from mitochondrial heme-copper oxidases. Nature Communications 2022 13:1 [Internet]. 2022 Dec 8 [cited 2025 Jul 13];13(1):1–14. Available from: https://www.nature.com/articles/s41467-022-34771-y
30. Jung W, Panda A, Lee J, Ghosh S, Shaw JB, Gupta K. Native Top–Down Analysis of Membrane Protein Complexes Directly From In Vitro and Native Membranes. Molecular & Cellular Proteomics [Internet]. 2025 Jul 1 [cited 2025 Aug 18];24(7):100993. Available from: https://www.sciencedirect.com/science/article/pii/S153594762500091X?pes=vor&utm_source=acs&getft_integrator=acs#bib76
31. Ventouri IK, Malheiro DBA, Voeten RLC, Kok S, Honing M, Somsen GW, et al. Probing Protein Denaturation during Size-Exclusion Chromatography Using Native Mass Spectrometry. Anal Chem [Internet]. 2020 Mar 17 [cited 2025 Aug 18];92(6):4292–300. Available from: https://pmc.ncbi.nlm.nih.gov/articles/PMC7081181/
32. Otzen DE. Protein unfolding in detergents: Effect of micelle structure, ionic strength, pH, and temperature. Biophys J [Internet]. 2002 Oct 1 [cited 2025 Aug 18];83(4):2219–30. Available from: https://www.cell.com/action/showFullText?pii=S0006349502739829
33. Laganowsky A, Reading E, Hopper JTS, Robinson C V. Mass Spectrometry of Intact Membrane Protein Complexes. Nat Protoc [Internet]. 2013 Mar [cited 2025 Aug 18];8(4):639. Available from: https://pmc.ncbi.nlm.nih.gov/articles/PMC4058633/

Acknowledgements – I would like to express my sincere gratitude to Dr. Ye Gao for her supervision, daily guidance, and constructive feedback throughout this project, as well as for her support in reviewing my thesis. I am deeply thankful to Anjusha Mathew for her patience in teaching me and for her continuous help with native-MS experiments. I also gratefully acknowledge Prof. Ron Heeren for designing this project and providing me with the opportunity to carry it out as my thesis.I am thankful to the IDEE department of Maastricht University for assistance with spectrophotometry and to the Biochemistry Department for granting access to laboratory facilities and instrumentation. I would also like to thank Sneha Hake for her contributions to the experimental work and the M4I Nanoscopy group for their warm welcome during my internship.

Supplemental information

Table S1 – Manufacturers information for materials and instruments

Product	Brand	Ref number
E. *coli* C43 (DE3)	Thermo Fisher Scientific	N/A
LB-Broth Miller	FormediumTM LTD	LMM0102
Glycerol	Sigma-Aldrich	G5516-1L
Ampicillin sodium salt	Sigma-Aldrich	A9518-25G
Millex®-HV Sterile Filter Unit with Durapore® PVDF membrane (0.45µm)	Merck Milipore Ltd.	SLHVO33RB
IPTG, dioxane-free	Thermo Fisher Scientific	R0392
Trizma® base Tris buffer	Sigma-Aldrich	T1503-1kG
NaCl	Sigma-Aldrich	71380-5KG
Benzonase® Nuclease	EMD Milipore corp.	70746-3
cOmplete™ ULTRA Tablets, Mini, EDTA-free, EASYpack Protease Inhibitor Cocktail	Merck KGaA	5892791001
n-dodecyl-beta-D-maltodside (lauryl maltoside, DDM)	Glycon Biochemicals GmbH	CAS-69227-93-6
HisPur™ Ni-NTA Resin	Thermo Fisher Scientific	88222
Econo-Column® Chromatography Columns	Bio-Rad	#7372512
Imidazole	Sigma-Aldrich	I202-500G
Macrosep® Advance Centrifugal Device (30K MWCO)	Cytiva	89509A
Whatman™ membrane filter cellulose acetate (0.2µm)	Cytiva	10404112
Superose™ 6 Increase 3.2/300 SEC column	GE Healthcare Life Sciences (Cytiva)	29-0915-98
EXtrelut® NT1 Pre-packed columns	EMD Milipore corp.	1.15094.0001
Cyclohexane	Sigma-Aldrich	34855-1L-M
Ethanol	Sigma-Aldrich	1.00986.1000
Amicon® Ultra Centrifugal Filter (10 kDa MWCO)	Merck Milipore Ltd.	UFC5010

Instrument	Brand	Ref number
Multitron standard Shaker for 9 x 1 L culture	Infors HT	N/A
Avanti J-26 XP centrifuge with JLA-8.1000 rotor	Beckman Coulter Life Sciences	/
Centrifuge 5810 R with A-4-62 swing-bucket rotor	Eppendorf	Cat No° 5811000015
Centrifuge 5424R	Eppendorf	/
Optima XPN-90 Ultracentrifuge with 70Ti Rotor	Beckman Coulter Life Sciences	A94468

Stuart Roller Mixer SRT6	Thermo Fisher Scientific Scientific Ltd.	Cat No° SRT/STACK
RV5 Vacuum pump	Edwards	Serial No. 109448130
French press: EmulsiFlex-C3	Avestin inc.	serial# C315971
Nanodrop DS-11+ UV-Vis Spectrophotometer	DeNovix©	DS-11+
Shimadzu FPLC: DGU-20A_{5r} degassing unit, LC-20AD liquid chromatograph, SIL-20A auto sampler	Shimadzu Corp.	DGU-20A_{5r}, LC-20AD, SIL-20A